Journal of
Materials Chemistry A

PAPER

Cite this: *J. Mater. Chem. A*, 2014, **2**, 7570

Confined synthesis of ultrafine Ru–B amorphous alloy and its catalytic behavior toward selective hydrogenation of benzene†

Jie Liu, Shan He,* Changming Li, Fei Wang, Min Wei,* David G. Evans and Xue Duan

Received 2nd January 2014
Accepted 27th February 2014

DOI: 10.1039/c4ta00023d

www.rsc.org/MaterialsA

How to control the size and morphology of metal nanocatalysts is of vital importance in enhancing their catalytic performance. In this work, uniform and ultrafine Ru–B amorphous alloy nanoparticles (NPs) supported on titanate nanosheets were fabricated *via* a confined synthesis in titanate nanotubes (TNTs) followed by unwrapping the tube to sheetlike titanate (TNS) (denoted as Ru–B/TNS), which exhibit excellent catalytic performance toward the selective hydrogenation of benzene to cyclohexene (yield$_{\text{cyclohexene}}$: 50.7%) without any additives. HRTEM images show the resulting Ru–B NPs are highly dispersed on the titanate nanosheets (particle size: 2.5 nm), with a low Ru–Ru coordination number revealed by EXAFS. Moreover, XPS demonstrates the surface-enriched B element and a strong electron transfer from B to Ru, which facilitates the formation and desorption of cyclohexene on the Ru active-sites, accounting for the significantly enhanced catalytic behavior. The surfactant-free confined synthesis and additive-free catalytic system make the Ru–B/TNS catalyst a promising candidate for the selective hydrogenation of benzene.

1. Introduction

Amorphous alloy catalysts have attracted considerable attention from both academia and industry owing to their higher activity, better selectivity and stronger corrosion resistance in many important hydrogenation reactions in comparison with their crystalline catalytic equivalents.[1–4] One of the most widely studied amorphous alloys has been M–B (M = Ru, Ni, Co), which is generally obtained *via* the direct reduction of the M ions by borohydride (BH_4^-) in aqueous solution.[5–9] However, the as-prepared M–B amorphous alloy catalysts often suffer from severe aggregation as a result of the vigorous and strong exothermic reduction process, significantly depressing their catalytic performance. Although many endeavors have been devoted to preparing uniform amorphous alloys, the use of a large amount of toxic organic reagents as well as the resulting large size of the M–B nanoparticles (NPs) are inevitable.[10–13] Therefore, how to achieve mono-dispersed and ultrafine M–B amorphous alloy catalysts is important and remains a challenging goal by the use of conventional synthetic methods.

Titanate nanotubes (TNTs), a new class of versatile material, have been studied as supports in catalysis and separation due to their unique structural properties.[14–18] Typically, this material can be synthesized *via* a simple alkaline hydrothermal treatment of TiO_2,[19,20] possessing an abundant and uniform mesoporous structure. One of the most interesting features of this material is the structural transformation from tubular to sheet titanate after an acid–alkaline treatment, as reported by Teng and Tsai.[21] It is well known that mesoporous materials, such as molecular sieves and carbon nanotubes, are often used as supports to provide a confined growth environment for the preparation of well-defined and uniform-sized nanocatalysts.[22–25] Regarding the TNT material, its instinctive mesoporous structure, similar to that of typical mesoporous materials mentioned above, mean it could also be used as a support to provide a confined environment for the preparation of nanocatalysts. Importantly, this confined environment is expected to be removed by virtue of the tube-to-sheet structural transformation after the confined synthesis of the nanocatalyst, so as to enhance the mass diffusion process. Inspired by the unique structure of the TNT material, a promising idea is proposed here that size-controlled M–B amorphous alloy catalysts with fully exposed active-sites could be fabricated based on the confined synthesis in titanate nanotubes followed by unwrapping the tube to sheetlike titanate for unconfined catalysis.

In this work, we report the fabrication of an ultrafine and uniform Ru–B amorphous alloy nanocatalyst supported on titanate nanosheets *via* a facile two-step procedure involving the confined synthesis of Ru–B NPs in titanate nanotubes followed by a structural transformation from tubular to sheetlike titanate (Scheme 1), which exhibits excellent catalytic

---

State Key Laboratory of Chemical Resource Engineering, Beijing University of Chemical Technology, Beijing 100029, P. R. China. E-mail: vh30@163.com; weimin@mail.buct.edu.cn

† Electronic supplementary information (ESI) available: Additional characterization results are included. See DOI: 10.1039/c4ta00023d

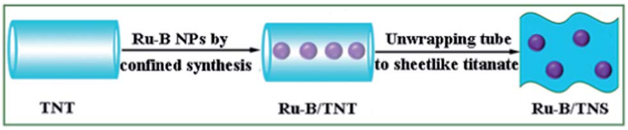

Scheme 1 Illustration for the synthesis of ultrafine Ru–B amorphous alloy nanoparticles supported on sheetlike titanate (TNS).

performance (yield$_{cyclohexene}$: 50.7%) for the selective hydrogenation of benzene to cyclohexene without any additives. In addition, the manufacture of cyclohexene in this work demonstrates an additive-free process, superior to traditional additive-dependent catalytic systems in terms of equipment corrosion and subsequent separation. HRTEM images show that the resulting Ru–B NPs with a small size (2.5 nm) are highly dispersed on the titanate nanosheet. EXAFS demonstrates that the ultrafine Ru–B NPs exhibit a high level of Ru unsaturation. XPS further reveals a large density of surface alloying B and a strong electron transfer from B to Ru. This is favorable for the formation and desorption of cyclohexene, accounting for the largely enhanced yield of cyclohexene over the Ru–B/TNS catalyst. Our approach holds significant promise for the design and fabrication of an ultrafine Ru–B amorphous alloy nanocatalyst, which can serve as a promising candidate in hydrogenation reactions.

2. Experimental section

2.1 Materials

$RuCl_3 \cdot 3H_2O$ and TiO_2 (anatase) were purchased from Sigma-Aldrich. Other chemicals, including NaOH, HCl, $NaBH_4$, benzene, cyclohexene, and cyclohexane were purchased from the Beijing chemical Co., LTD, and used without further purification. Deionized water was used in all experimental processes.

2.2 Fabrication of the Ru–B catalyst

Synthesis of Ru–B nanoparticles within titanate nanotubes (Ru–B/TNTs). Firstly, titanate nanotubes (TNTs) were obtained from an alkaline hydrothermal treatment of TiO_2 described by Kasuga *et al.*[19] Typically, 3.0 g of TiO_2 was dispersed in NaOH solution (120 mL, 10 M) and placed in a Teflon-lined stainless-steel autoclave at 150 °C for 24 h. The precipitation was washed with HCl solution (0.1 M) and deionized water until $\mathrm{pH} = \sim 8$, and then dried in an air circulating oven at 80 °C for 8 h, yielding the TNTs. Secondly, by utilizing the confinement effect of the tubular titanate, size-controlled Ru–B NPs were prepared. In detail, TNTs (1.0 g) were added into acetone solution (40 mL) containing $RuCl_3 \cdot 3H_2O$ (0.0506 g) under vigorous stirring followed by ultrasonication for 1 h. The obtained suspension was dried under ambient conditions to allow slow evaporation of acetone, and then dried at 80 °C for 5 h with a heating rate of 1 °C $\mathrm{min^{-1}}$. The final solid was added into $NaBH_4$ aqueous solution (40 mL; 15 mg $\mathrm{mL^{-1}}$) under vigorous stirring and aged for 30 min. The obtained suspension was centrifuged, washed thoroughly and dried in a vacuum oven at 50 °C for 12 h, and denoted Ru–B/TNTs.

Preparation of Ru–B/TNS catalyst. The Ru–B/TNS catalyst was derived from the Ru–B/TNTs sample based on the structural transformation process.[21] In detail, the as-synthesized Ru–B/TNTs precursor (0.5 g) was added into water (40 mL); 0.5 M HCl solution was added dropwise into the above slurry until a pH value of 0.38 was reached. After agitation for 12 h, the pH value of the resulting slurry was adjusted to 12 with NaOH solution (1.0 M). The obtained precipitation was separated, washed with deionized water until the pH reached 8.0, followed by drying at 50 °C in a vacuum oven for 12 h, yielding the Ru–B/TNS catalyst.

Preparation of Ru–B/TNT–IMP catalyst. As a reference sample, Ru–B/TNT–IMP was obtained by the conventional impregnation method according to the reported literature.[26] Typically, TNTs (1.0 g) were added into deionized water (40 mL) containing $RuCl_3 \cdot 3H_2O$ (0.0506 g) under vigorous stirring for 1 h. Afterwards 0.6 g of $NaBH_4$ was added into the above suspension. After agitation for 30 min, the resulting precipitation was centrifuged and washed thoroughly, followed by drying in a vacuum oven at 50 °C for 12 h, and denoted Ru–B/TNT–IMP.

Preparation of Ru–B/TNS–IMP catalyst. The TNS support was firstly derived from the TNT precursor. In detail, the TNT precursor (0.5 g) was added into water (40 mL), and then 0.5 M HCl solution was added dropwise into the above slurry until $\mathrm{pH} = 0.38$. After agitation for 12 h, the pH value of the resulting slurry was adjusted to 12 with NaOH solution (1.0 M). The obtained precipitation was separated and washed with deionized water until the pH reached 8, followed by drying at 60 °C for 12 h, yielding the TNS support. Finally, the Ru–B/TNS–IMP catalyst was prepared by the impregnation method[26] similar to the sample of Ru–B/TNT–IMP mentioned above.

2.3 Catalytic evaluation toward the selective hydrogenation of benzene to cyclohexene

The selective hydrogenation of benzene was performed in a Teflon-lined stainless steel autoclave (100 mL) equipped with a magnetic stirrer. In a typical experiment, 10 mL of benzene, 0.05 g of catalyst, and 20 mL of water were introduced into the reactor. After being purged by low pressure hydrogen four times to remove air, the reactor was heated to the reaction temperature. Then hydrogen was added into the reactor until the desired pressure was reached. The products were analyzed using a gas chromatograph (GC-2014C) equipped with a flame ionization detector (FID) and a PEG-20 M capillary column (0.25 mm in diameter, 30 m in length).

To test the reusability, the Ru–B/TNS catalyst was separated from the liquid by centrifugation, washed thoroughly and dried under vacuum at 50 °C for 5 h, followed by direct reuse for the next run without further reduction.

2.4 Characterization

X-ray diffraction (XRD) patterns of the samples were obtained on a Rigaku XRD-6000 diffractometer, using Cu Kα radiation

($\lambda = 0.154$ nm) at 40 kV, 40 mA, a scanning rate of 10° min^{-1}, a step size of 0.02° s^{-1}, and a 2θ angle ranging from 3 to 80°. Narrow range XRD patterns were scanned from 40° to 50° at 1° min^{-1}. Elemental analysis of the Ru–B amorphous alloy was performed using a Shimadzu ICPS-7500 inductively coupled plasma emission spectrometer (ICP-ES). High-resolution electron microscopy (HRTEM) observations were carried out on a JEM-2100 transmission electron microscope. X-ray photoelectron spectroscopy (XPS) was recorded on a Thermo VG Escalab 250 X-ray photoelectron spectrometer at a pressure of $\sim 2 \times 10^{-9}$ Pa with Al Kα X-rays as the excitation source. The vacuum Fourier transform infrared (FTIR) spectra were recorded using a Vector22 (Bruker) spectrophotometer in the range 4000–400 cm^{-1} with 2 cm^{-1} of resolution under 10^{-8} Pa vacuum. The standard KBr disk method (1 mg of sample in 100 mg of KBr) was used. Low-temperature N_2 adsorption–desorption isotherms of the samples were obtained on a Quantachrome Autosorb-1C-VP instrument. The sample was outgassed prior to analysis at 100 °C for 12 h under 10^{-4} Pa vacuum. The total specific surface area was evaluated from the multipoint Brunauer–Emmett–Teller (BET) method. The hydrogenation temperature programmed desorption (H_2-TPD) measurements were conducted in a quartz tube reactor on a Micromeritics ChemiSorb 2720 with a thermal conductivity detector (TCD). Typically, 100 mg of sample was first sealed and degassed under flowing Ar at 200 °C for 2 h, then cooled down to room temperature for adsorption of H_2 for 1 h. Afterwards, the sample was purged in Ar to remove the physically adsorbed H_2 for 30 min. Finally, the sample was placed in a stream of Ar with a rate of 40 mL min^{-1} and a temperature ramp of 10 °C min^{-1} to perform the TPD measurement.

3. Results and discussion

3.1 Structural and electronic properties

Fig. 1A shows the powder XRD patterns of the bare TNTs and the Ru–B catalysts supported on titanate. For the bare TNTs, typical (200), (110) and (310) reflections at ~10°, 24° and 28° were observed, which can be indexed to body-centered orthorhombic titanate (JCPDS no. 47-0124). Compared with the TNTs, the samples of Ru–B/TNTs and Ru–B/TNS display a similar titanate phase, without any reflections of the Ru–B amorphous alloy, implying a high dispersion or low concentration of Ru–B NPs (below the detection limit of XRD). In contrast, for the two Ru–B catalysts prepared by the impregnation (IMP) method (Ru–B/TNT–IMP and Ru–B/TNS–IMP), an extra weak reflection at ~44° was observed, which can be indexed to the typical Ru–B amorphous alloy phase.[27,28] This was further confirmed by the narrow-range XRD patterns scanned from 40° to 50° (Fig. 1B). The results indicate a larger particle size of Ru–B NPs prepared by the IMP method than that by the confined synthesis.

The TEM images (Fig. 2a and b) clearly show the multi-walled and open-ended structure of the TNTs, with an inner diameter of ~5 nm and wall interspacing of ~0.78 nm, in accordance with those reported in the literature.[29,30] After loading Ru–B NPs on the TNTs by the confined method, the TEM images of the resulting Ru–B/TNTs sample (Fig. 2c and d) show uniform and small nanoparticles (~2.5 nm) accommodated in the tube channels of the TNTs. After unwrapping the tubular support, the resulting Ru–B/TNS (Fig. 2e) clearly exhibits uniform nanoparticles (2.5 ± 0.3 nm) formerly confined in the TNTs which are exposed and highly dispersed on the sheetlike titanate support. The HRTEM and SAED images (Fig. 2f and g) further reveal a long-range disordered but short-range ordered structure with a diffraction halo for a single

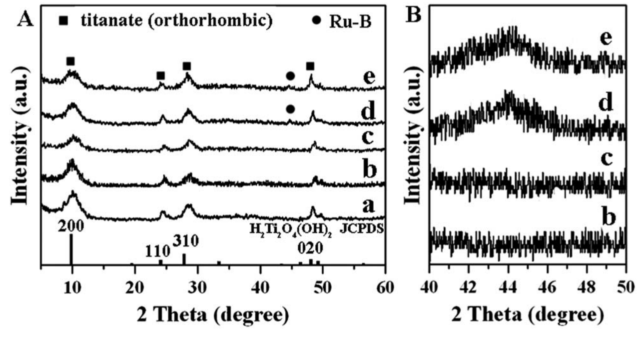

Fig. 1 (A) Wide-range and (B) narrow-range XRD patterns of: (a) TNTs, (b) Ru–B/TNTs, (c) Ru–B/TNS, (d) Ru–B/TNT–IMP, (e) Ru–B/TNS–IMP.

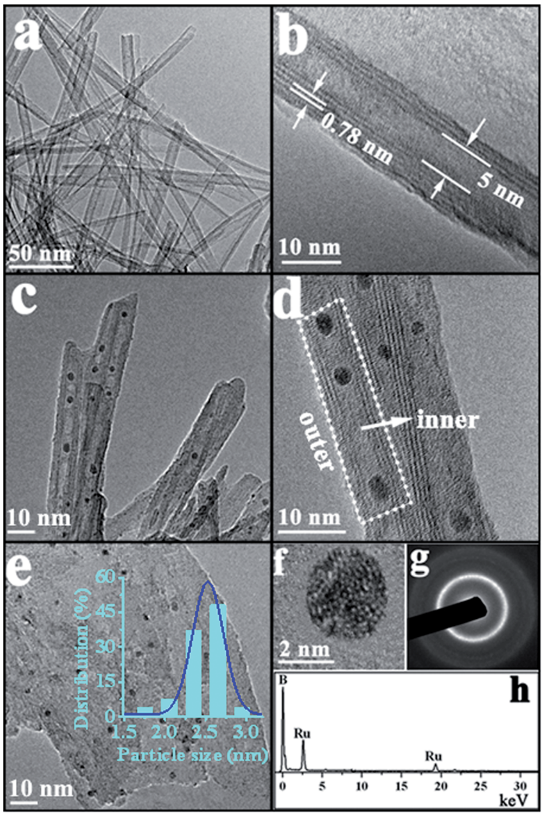

Fig. 2 (a and b) TEM and HRTEM images of pristine TNTs, (c and d) Ru–B/TNTs at low and high magnification, (e) Ru–B/TNS with size-distribution shown in the inset (300 particles analyzed), (f and g) HRTEM and SAED images of a single Ru–B particle, (h) EDS results of Ru–B particles.

nanoparticle, indicative of a typical amorphous alloy.[31] EDS analysis (Fig. 2h) shows the nanoparticles are composed of Ru and B elements, implying the presence of a Ru–B amorphous alloy. This will be further confirmed by the XPS technique below. The merit of this confined synthesis approach is further illuminated by comparison with the conventional IMP method. For the Ru–B/TNT–IMP sample, the Ru–B particles suffer from severe aggregation, randomly stacking on the exterior surface of the TNTs with a broad size distribution (21.2 ± 6.0 nm) (Fig. S1a and b†); similar aggregation was also observed in the Ru–B/TNS–IMP sample after unfolding the tubes (Fig. S1c†). H_2-TPD further showing that the confine-synthesized samples have a higher Ru dispersion than the IMP ones (Fig. S2† and Table 1).

However, it should be noted that the solvent acetone is necessary for the confined synthesis of Ru–B nanoparticles. If water was used as the solvent, the resulting Ru–B particles would also load on the external surface of the TNTs with serious aggregation (Fig. S3†). This can be explained by the lower surface tension of acetone in comparison with water,[33] which facilitates the migration of the ruthenium precursor into the interior channels of the TNTs *via* capillary force. Therefore, the results demonstrate that ultrafine and uniform Ru–B NPs can be successfully obtained by confined synthesis in TNTs. Moreover, taking advantage of the structural transformation from tube to sheet titanate, the resulting Ru–B NPs are fully exposed on the outer surface of the TNS support.

Fig. 3 displays the N_2 adsorption–desorption isotherms and BJH pore size distributions of the TNTs, Ru–B/TNTs and Ru–B/TNS. The isotherms for the TNTs and Ru–B/TNTs show a distinct hysteresis loop, indicating a high density of mesopores in the two samples (type-IV according to IUPAC classification). For the sample of Ru–B/TNS, a weak hysteresis loop is also observed, implying the existence of mesopores possibly resulting from the interspace between titanate nanosheets. The inset shows that the TNTs and Ru–B/TNTs have a narrow pore size distribution, ranging from 3–10 nm with a peak located at ~5 nm, in accordance with the TEM results (Fig. 2). However, a largely decreased pore volume for the Ru–B/TNS sample was observed, owing to the formation of the sheetlike support.[34] In addition, it should be noted that all the supported Ru–B catalysts have a large specific surface area (>200 $m^2\ g^{-1}$, Table 1), which is favorable to their catalytic performance.[35]

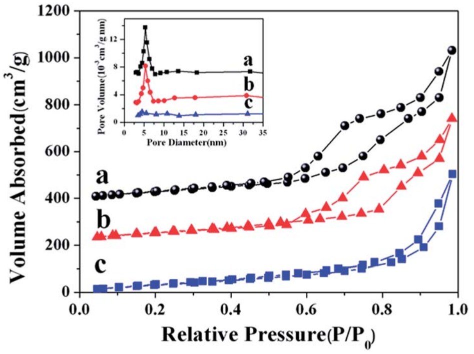

Fig. 3 N_2 adsorption–desorption curves and pore size distributions (inset) of (a) TNTs, (b) Ru–B/TNTs, (c) Ru–B/TNS.

X-ray photoelectron spectroscopy (XPS) was employed to analyze the chemical environment of the supported Ru–B NPs on titanate (Fig. 4). One peak at 280.0 eV (Ru $3d_{5/2}$) is observed for all four samples (Fig. 4, curves a_1–d_1), indicating the presence of a metallic state for Ru.[36] The B species exhibits both a high BE value (192.0 eV) and a low one (188.5 or 188.0 eV) (Fig. 4, curves a_2–d_2), which are attributed to the oxidized and elemental state,[37] respectively. The BE value of B in all the samples exceeds that of pure B (187.1 eV), further implying the formation of a Ru–B amorphous alloy in which electron transfer may occur from B to Ru. However, no obvious BE shift for the metallic Ru can be observed, possibly due to its much larger atomic weight compared with the B atom.[37,38] Interestingly, the Ru–B/TNTs and Ru–B/TNS samples exhibit a higher BE value of B1s (188.5 eV) than that of the IMP ones (188.0 eV), implying a stronger Ru–B interaction in the confined synthesis. In addition, the XPS analysis also demonstrates that the confine-synthesized samples exhibit a higher B : Ru molar ratio on the surface (~35/65) than the IMP ones (~20/80), although the ICP results reveal a similar bulk composition for all these Ru–B samples (see Table 1). This implies that the ultrafine Ru–B NPs by the confined synthesis are surface-enriched with alloying B.[39]

To obtain a deeper insight into the as-prepared Ru–B samples, the coordination structure of the Ru atom in the Ru–B NPs was further characterized by extended X-ray absorption fine structure (EXAFS) spectroscopy (Fig. 5). The fitting parameters (Table 2) show that the Ru–Ru coordination numbers of all these Ru–B samples are less than that of Ru foil (12.4). Moreover, the Ru–B/TNTs and Ru–B/TNS exhibit a lower Ru–Ru coordination number (4.2) than the IMP ones (6.8), *i.e.*, the Ru–B NPs obtained by the confined synthesis possess a higher unsaturation of Ru species. It is well known that some metalloids (*e.g.*, B or P) should be incorporated for the formation and

Table 1 Structural parameters of various samples

Samples	S_{BET} ($m^2\ g^{-1}$)	Ru[a] (wt%)	Bulk molar ratio[a]	Surface molar ratio[b]	Ru dispersion[c] (%)	Mean Ru–B particle size by TEM (nm)
TNTs	246	—	—	—	—	—
Ru–B/TNTs	232	1.95	$Ru_{72.1}\ B_{27.9}$	$Ru_{65.2}\ B_{34.8}$	65.9	2.5 ± 0.4
Ru–B/TNS	212	1.95	$Ru_{72.0}\ B_{28.0}$	$Ru_{64.9}\ B_{35.1}$	66.2	2.5 ± 0.4
Ru–B/TNT–IMP	227	1.96	$Ru_{71.3}\ B_{28.7}$	$Ru_{80.1}\ B_{19.9}$	19.6	21.2 ± 6.0
Ru–B/TNS–IMP	203	1.97	$Ru_{71.4}\ B_{28.6}$	$Ru_{81.1}\ B_{18.9}$	20.1	20.1 ± 5.8

[a] Values determined by ICP. [b] Values determined by XPS. [c] Values based on the H_2-TPD results.[32]

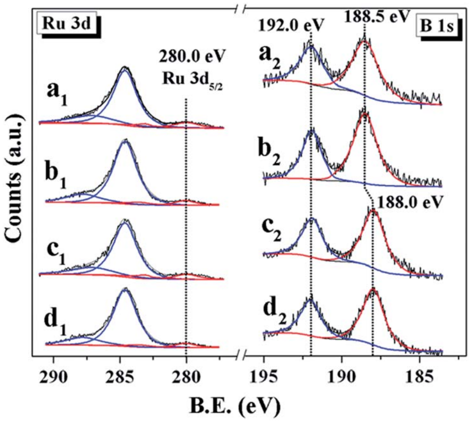

Fig. 4 XPS spectra of Ru 3d and B 1s for: (a_1 and a_2) Ru–B/TNTs, (b_1 and b_2) Ru–B/TNS, (c_1 and c_2) Ru–B/TNT–IMP, and (d_1 and d_2) Ru–B/TNS–IMP.

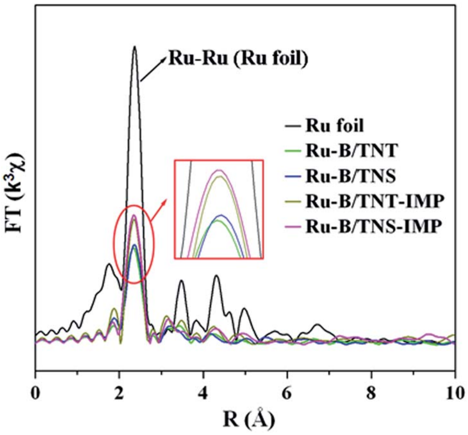

Fig. 5 Fourier transforms of EXAFS spectra for Ru foil, Ru–B/TNTs, Ru–B/TNS, Ru–B/TNT–IMP and Ru–B/TNS–IMP.

Table 2 EXAFS fitting parameters of various samples[a]

Samples	*N*	*R* (Å)
Ru foil	12.4	2.67
Ru–B/TNTs	4.2	2.67
Ru–B/TNS	4.2	2.67
Ru–B/TNT–IMP	6.8	2.67
Ru–B/TNS–IMP	6.8	2.67

[a] *N* = coordination number. Error bounds (accuracies) characterizing the structural parameters obtained by EXAFS are estimated as follows: coordination number *N*, ±20%; distance *R*, ±0.02 Å.

stabilization of the amorphous structure of metastable materials.[5,6] Higher unsaturation of Ru in Ru–B/TNS indicates a larger surface free energy, which induces the enrichment of B atoms on the surface.

3.2 Catalytic performance tests

The catalytic performances of the as-synthesized Ru–B catalysts were evaluated by the selective hydrogenation of benzene to cyclohexene, which is an important chemical intermediate for producing value-added cyclohexanol, adipic acid and caprolactam.[40–43] Fig. 6 shows the content plots of benzene, cyclohexene and cyclohexane as a function of reaction time over the as-prepared Ru–B catalysts (reaction temperature: 150 °C; H_2

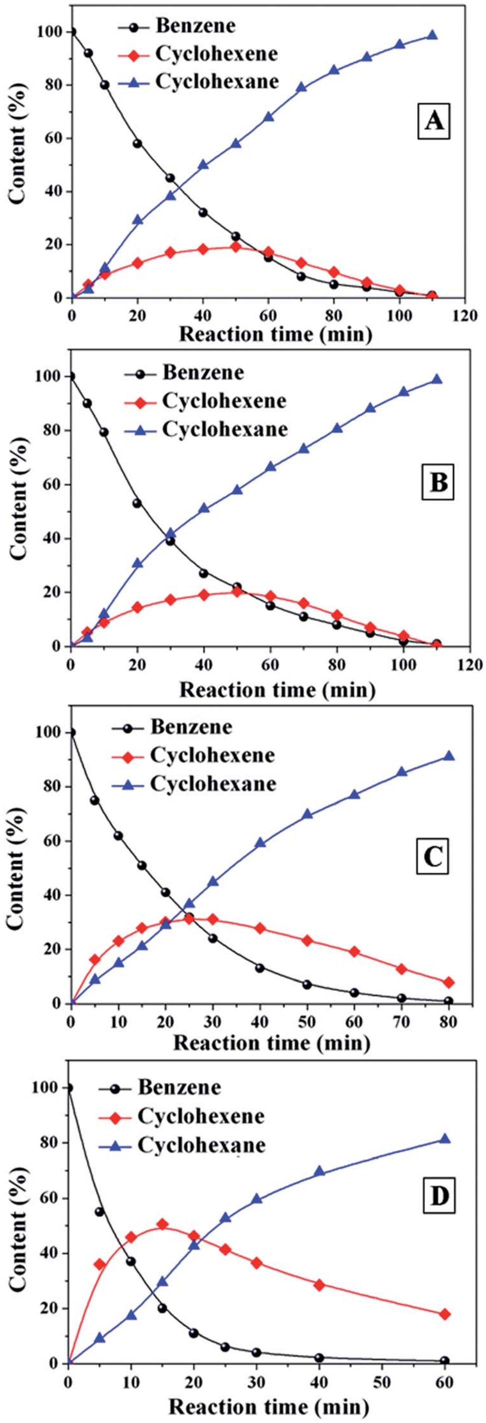

Fig. 6 The time courses of benzene hydrogenation over the Ru–B catalysts: (A) Ru–B/TNT–IMP, (B) Ru–B/TNS–IMP, (C) Ru–B/TNTs, (D) Ru–B/TNS. Reaction conditions: catalyst (0.05 g), benzene (10 mL), H_2O (20 mL), temperature (150 °C), H_2 pressure (5.0 MPa), stirring rate (1000 rpm).

pressure: 5.0 MPa). It can be seen that the benzene content decreases gradually and the completely saturated product cyclohexane increases monotonically along with reaction time. Regarding the cyclohexene content, a maximum is obtained at a certain reaction time, exhibiting the well-known behavior of consecutive reactions. Among the as-prepared Ru–B catalysts, Ru–B/TNT–IMP and Ru–B/TNS–IMP show a relatively low yield of cyclohexene (19.2% and 20.3%, respectively) while the Ru–B/TNTs catalyst displays an increase in yield (31.3%). Interestingly, after further unwrapping the tubes to sheet titanate, the resulting Ru–B/TNS catalyst exhibits a significantly enhanced yield of 50.7%, which is among the highest value compared with previous reports.[44] Moreover, the reaction occurs faster over the Ru–B/TNS catalyst (the maximum yield of cyclohexene: 50.7% at 15 min) than over the Ru–B/TNTs one (the maximum yield of cyclohexene: 31.3% at 25 min) (Fig. 6C and D), indicating improved reaction dynamics.

To provide further understanding of the marked difference in the yield of cyclohexene, the turnover frequency (TOF) of benzene over these catalysts was calculated based on the weigh-specific activity (R_0) and the dispersion degree of Ru. As shown in Table 3, the TOF value of benzene over the Ru–B/TNS catalyst is highest (26.5 s^{-1}), almost twice that of Ru–B/TNTs and three times that of Ru–B/TNT–IMP and Ru–B/TNS–IMP. It is well known that metal catalysts with high unsaturation have generally been proved to show excellent hydrogenation activity.[45] Compared to the Ru–B/TNT–IMP and Ru–B/TNS–IMP catalysts, by utilizing the confined synthesis, an ultrafine Ru–B catalyst was obtained, which effectively catalyzes benzene hydrogenation due to its high Ru unsaturation revealed by EXAFS. In addition, in this tetra-phase catalytic reaction, the diffusion of benzene plays an important role in the hydrogenation conversion.[46] Fig. S4† shows the benzene conversion as a function of reaction time. It can be seen that the reaction rate over the Ru–B/TNS catalyst increases significantly in comparison with Ru–B/TNTs, based on its enhanced slope of the conversion-time plot at the half conversion of benzene.[47] This can be explained by the markedly decreased inner diffusion resistance of benzene as a result of the tube–sheet structural transformation of the support. These features account for the highest TOF value of benzene over the Ru–B/TNS catalyst.

The nature of the ultrafine Ru–B NPs and the sheetlike support also impose significant impact on the selectivity to cyclohexene. As can be seen in Table 3, Ru–B/TNS exhibits the largest cyclohexene selectivity. It was reported that benzene adopts a π-mode adsorption configuration on Ru[48,49] and its complete hydrogenation to cyclohexane depends on the appropriate number of neighboring surface sites as surface-enriched alloying B may favor the formation of cyclohexene. Moreover, the desorption of cyclohexene could be facilitated due to the enhanced repulsive interaction between electron-enriched Ru and the C═C bond in cyclohexene[49] as well as the decreased diffusion resistance of cyclohexene from Ru active-sites to the oil phase after the tube–sheet structural transformation of titanate. Consequently, a high yield of cyclohexene was obtained over the Ru–B/TNS catalyst due to the above simultaneously enhanced conversion and selectivity. To the best of our knowledge, the same level of cyclohexene yield

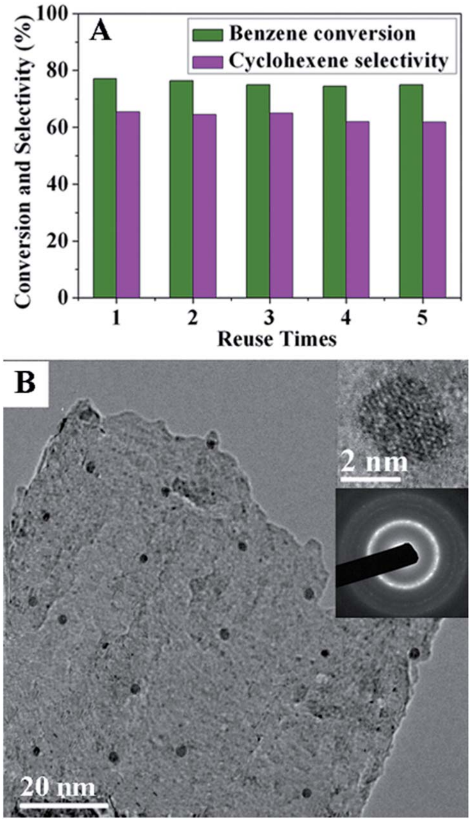

Fig. 7 (A) The catalytic performances of Ru–B/TNS in 5 consecutive recycles. (B) The TEM image of the Ru–B/TNS sample after five cycles of reuse (the insets show the HRTEM and SAED image of a single Ru–B particle).

Table 3 Catalytic performance of various Ru–B catalysts[a]

Catalysts	t^b (min)	Conv.^{b} (%)	$S_{CHE}{}^b$ (%)	$Y_{CHE}{}^b$ (%)	$R_0{}^c$ (mol min^{-1} g^{-1})	TOF (s^{-1})
Ru–B/TNT–IMP	50.0	56.9	33.7	19.2	0.022	9.6
Ru–B/TNS–IMP	50.0	58.6	34.6	20.3	0.025	9.8
Ru–B/TNTs	25.0	67.8	46.2	31.3	0.112	14.4
Ru–B/TNS	15.0	80.1	63.3	50.7	0.203	26.5

[a] Reaction conditions: catalyst 50 mg, benzene 10 mL, H_2O 20 mL, H_2 pressure 5.0 MPa, reaction temperature 150 °C. [b] The results are provided at the maximum yield of cyclohexene. Conv. = conversion of benzene; S_{CHE} = selectivity to cyclohexene; Y_{CHE} = yield of cyclohexene. [c] Value was calculated based on the amount of converted benzene per minute per gram of catalyst.

reported in previous studies generally involves both a Ru catalyst and a high amount of inorganic additives (*e.g.*, $ZnSO_4$), resulting in problems of reactor corrosion and separation. In comparison, herein the employment of the as-synthesized ultrafine and highly-dispersive Ru–B catalyst offers a facile and green route for the selective hydrogenation of benzene. In addition, the Ru–B/TNS catalyst exhibits a good reusability; its activity and selectivity toward cyclohexene remains almost unchanged in five recycles (Fig. 7A). The TEM images further reveal that the particle size and morphology of the used catalyst can be maintained (Fig. 7B), demonstrating a stable, effective and recyclable catalyst.

4. Conclusion

In summary, highly-dispersed Ru–B NPs supported on sheet-like titanate were fabricated *via* a two-step method. The spatial effect of the tubular titanate induces the formation of ultrafine Ru–B NPs in the confined synthesis; the subsequent structural transformation of support from nanotube to nanosheet provides an unconfined environment for the selective hydrogenation of benzene to cyclohexene, eliminating the internal diffusion resistance. The resulting Ru–B NPs with surface-enriched alloying B and electron-enriched Ru species, account for the superior catalytic behavior. This work provides a facile approach for the design and fabrication of a supported Ru–B amorphous alloy nanocatalyst, which can serve as a promising candidate in hydrogenation reactions.

Acknowledgements

This work was supported by the 973 Program (Grant no. 2011CBA00504), the National Natural Science Foundation of China (NSFC), the Scientific Fund from Beijing Municipal Commission of Education (20111001002) and the Fundamental Research Funds for the Central Universities (ZD 1303). M. Wei particularly appreciates the financial aid from the China National Funds for Distinguished Young Scientists of the NSFC.

Notes and references

1 (*a*) K. Klement, R. H. Willens and P. Duwez, *Nature*, 1960, **187**, 869; (*b*) J. Van Wonterghem, S. Mørup, C. J. W. Koch, S. W. Charles and S. Well, *Nature*, 1986, **322**, 622.

2 A. Molnar, G. V. Smith and M. Bartok, *Adv. Catal.*, 1989, **36**, 329.

3 J. F. Deng, J. Yang and S. S. Sheng, *J. Catal.*, 1994, **150**, 434.

4 H. L. Wang, J. M. Yan, Z. L. Wang, S. I. O and Q. Jiang, *J. Mater. Chem. A*, 2013, **1**, 14957.

5 J. F. Deng, H. X. Li and W. Wang, *J. Catal.*, 1999, **51**, 113.

6 Y. Chen, *Catal. Today*, 1998, **44**, 3.

7 H. X. Li, Y. Wu, H. Luo, M. Wang and Y. Xu, *J. Catal.*, 2003, **214**, 15.

8 G. Luo, S. R. Yan, M. H. Qiao, J. H. Zhuang and K. N. Fan, *Appl. Catal., A*, 2004, **275**, 95.

9 S. H. Xie, M. H. Qiao, H. X. Li, W. J. Wang and J. F. Deng, *Appl. Catal., A*, 1999, **176**, 129.

10 S. J. Chiang, B. J. Liaw and Y. Z. Chen, *Appl. Catal., A*, 2007, **319**, 144.

11 H. Li, J. Liu, S. H. Xie, M. H. Qiao, W. L. Dai and H. X. Li, *J. Catal.*, 2008, **259**, 104.

12 Z. H. Zhu, J. Q. Ma, L. Xu, L. Xu, H. X. Li and H. Li, *ACS Catal.*, 2012, **2**, 2119.

13 H. Li, Y. Wang, Q. F. Zhao and H. X. Li, *Res. Chem. Intermed.*, 2009, **35**, 779.

14 X. Han, Y. H. Zhu, X. L. Yang and C. Z. Li, *J. Alloys Compd.*, 2010, **500**, 247.

15 K. P. Yu, W. Y. Yu, M. C. Kuo, Y. C. Liou and S. H. Chien, *Appl. Catal., B*, 2008, **84**, 112.

16 (*a*) A. Danon, K. Bhattacharyya, B. K. Vijayan, J. L. Lu, D. J. Sauter, K. A. Gray, P. C. Stair and E. Weitz, *ACS Catal.*, 2012, **2**, 45; (*b*) S. D. Perera, R. G. Mariano, K. Vu, N. Nour, O. Seitz, Y. Chabal and K. J. Balkus, *ACS Catal.*, 2012, **2**, 949.

17 C. K. Lee, S. S. Liu, L. C. Juang, C. C. Wang, M. D. Lyu and S. H. Hung, *J. Hazard. Mater.*, 2007, **148**, 756.

18 E. Wada, M. Kitano, K. Nakajima and M. Hara, *J. Mater. Chem. A*, 2013, **1**, 12768.

19 (*a*) T. Kasuga, M. Hiramatsu, A. Hoson, T. Sekino and K. Niihara, *Langmuir*, 1998, **14**, 3160; (*b*) T. Kasuga, M. Hiramatsu, A. Hoson, T. Sekino and K. Niihara, *Adv. Mater.*, 1999, **11**, 1307.

20 X. M. Sun and Y. D. Li, *Chem.–Eur. J.*, 2003, **9**, 2229.

21 C. C. Tsai and H. Teng, *Chem. Mater.*, 2006, **18**, 367.

22 (*a*) C. Pham-Huu, N. Keller, C. Estournes, G. Ehret and M. J. Ledoux, *Chem. Commun.*, 2002, 1882; (*b*) W. Chen, Z. Fan, L. Gu, X. H. Bao and C. L. Wang, *Chem. Commun.*, 2010, **46**, 3905.

23 G. A. Du, S. Y. Lim, Y. H. Yang, C. Wang, L. Pfefferle and G. L. Haller, *J. Catal.*, 2007, **249**, 370.

24 D. U. Lee, B. J. Kim and Z. W. Chen, *J. Mater. Chem. A*, 2013, **1**, 4754.

25 M. I. Clerc, D. Bazin, M. D. Appay, P. Beaunier and A. Davidson, *Chem. Mater.*, 2004, **16**, 1813.

26 (*a*) S. C. Liu, Z. Y. Liu, Z. Wang, S. H. Zhao and Y. M. Wu, *Appl. Catal., A*, 2006, **313**, 49; (*b*) G. Y. Fan, W. D. Jiang, J. B. Wang, R. X. Li, H. Chen and X. J. Li, *Catal. Commun.*, 2008, **10**, 98.

27 A. Yokoyama, H. Komiyama, H. Inoue, T. Masumoto and H. M. Kimura, *J. Catal.*, 1981, **68**, 355.

28 H. B. Guo, H. X. Li, J. Zhu, W. H. Ye, M. H. Qiao and W. L. Dai, *J. Mol. Catal. A: Chem.*, 2003, **200**, 213.

29 G. H. Du, Q. Chen, R. C. Che, Z. Y. Yuan and L. M. Peng, *Appl. Phys. Lett.*, 2001, **79**, 3702.

30 B. D. Yao, Y. F. Chan, X. Y. Zhang, W. F. Zhang, Z. Y. Yang and N. Wang, *Appl. Phys. Lett.*, 2003, **82**, 281.

31 K. S. Martens, J. A. Parton, R. Vercruysse, K. Jacobs and P. A. Maier, *Catal. Lett.*, 1996, **38**, 209.

32 F. Z. Zhang, J. L. Chen, P. Chen, Z. Y. Sun and S. L. Xu, *AIChE J.*, 2012, **58**, 1853.

33 C. F. Wang, S. J. Guo, X. L. Pan, W. Chen and X. H. Bao, *J. Mater. Chem.*, 2008, **18**, 5782.

34 M. Kitano, E. Wada, K. Nakjima, S. Hayashi, S. Miyazaki, H. Kobayashi and M. Hara, *Chem. Mater.*, 2013, **25**, 385.

35 Y. F. Liu, B. D. Tymowski, F. Vigneron, L. Florea, O. Ersen, C. Meny, P. Nguyen, C. Pham, F. Luck and C. Pham-Huu, *ACS Catal.*, 2013, **3**, 393.

36 (*a*) J. C. Fuggle, T. E. Madey, M. Steinkilberg and D. Menzel, *Surf. Sci.*, 1975, **52**, 521; (*b*) C. M. Li, S. T. Zhang, B. S. Zhang, D. S. Su, S. He, Y. F. Zhao, J. Liu, F. Wang, M. Wei, D. G. Evans and X. Duan, *J. Mater. Chem. A*, 2013, **1**, 2461.

37 H. Li, H. X. Li, W. L. Dai, W. J. Wang, Z. G. Fang and J. F. Deng, *Appl. Surf. Sci.*, 1999, **152**, 25.

38 H. X. Li, H. Li, J. Zhang, W. L. Dai and M. H. Qiao, *J. Catal.*, 2007, **246**, 301.

39 H. X. Li, H. Li, W. L. Dai and M. H. Qiao, *Appl. Catal., A*, 2003, **238**, 119.

40 F. Schwab, M. Lucas and P. Claus, *Angew. Chem., Int. Ed.*, 2011, **50**, 10453.

41 F. Schwab, M. Lucas and P. Claus, *Green Chem.*, 2013, **15**, 646.

42 H. A. Smith and H. T. Meriwether, *J. Am. Chem. Soc.*, 1949, **71**, 413.

43 S. C. Liu, Z. Liu, Z. Wang, S. H. Zhao and Y. M. Wu, *Appl. Catal., A*, 2006, **313**, 49.

44 (*a*) H. Z. Liu, T. Jiang, B. X. Han, S. G. Liang, W. T. Wang, T. B. Wu and G. Y. Yang, *Green Chem.*, 2011, **13**, 1106; (*b*) J. L. Liu, Y. Zhu, J. Liu, Y. Pei, Z. H. Li, H. Li and H. X. Li, *J. Catal.*, 2009, **268**, 100; (*c*) H. Z. Liu, S. G. Liang, W. T. Wang, T. Jiang and B. X. Han, *J. Mol. Catal. A: Chem.*, 2011, **341**, 35.

45 R. T. Vang, K. Honkala, S. Dahl, E. K. Vestergaard, J. Schnadt, E. Laegsgaard, B. S. Clausen, J. K. Nørskov and F. Besenbacher, *Nat. Mater.*, 2005, **4**, 160.

46 J. L. Liu, L. J. Zhu, Y. Pei, J. H. Zhuang, H. Li, H. X. Li, M. H. Qiao and K. N. Fan, *Appl. Catal., A*, 2009, **353**, 282.

47 Q. Fu, W. X. Li, Y. X. Yao, H. Y. Liu, H. Y. Su, D. Ma, X. K. Gu, L. M. Chen, Z. Wang, H. Zhang, B. Wang and X. H. Bao, *Science*, 2010, **328**, 1141.

48 W. Braun, G. Held, H. P. Steinrück, C. Stellwag and D. Menzel, *Surf. Sci.*, 2001, **475**, 18.

49 C. Fan, Y. A. Zhu, X. G. Zhou and Z. P. Liu, *Catal. Today*, 2011, **160**, 234.